

This document is the unedited Author's version of a Submitted Work that was subsequently accepted for publication in Chemistry of Materials, copyright © American Chemical Society after peer review. To access the final edited and published work see:
<https://dx.doi.org/10.1021/acs.chemmater.7b03417>.

Unveiling a new high-temperature ordered magnetic phase in ϵ -Fe₂O₃

José Luis García-Muñoz¹, Arnau Romaguera¹, Francois Fauth², Josep Nogués^{3,4} and Martí Gich¹

¹ *Institut de Ciència de Materials de Barcelona, ICMAB-CSIC, Campus universitari de Bellaterra, E-08193 Bellaterra, Spain*

² *ALBA Synchrotron Light Facility, 08290 Cerdanyola del Vallès, Barcelona, Spain*

³ *Catalan Institute of Nanoscience and Nanotechnology (ICN2), CSIC and The Barcelona Institute of Science and Technology, Campus UAB, Bellaterra, 08193 Barcelona, Spain.*

⁴ *ICREA, Pg. Lluís Companys 23, 08010 Barcelona, Spain*

PACS numbers: 75.25.-j; 75.85.+t; 75.50.Vv ; 75.47.Lx ; 75.50.Tt ; 75.50.Gg ; 77.55.Nv

Abstract

Iron oxides are among the most abundant materials on earth and yet there are some of their basic properties which are still not well established. Here, we present temperature-dependent magnetic, X-ray and neutron diffraction measurements refuting the current belief that the magnetic ordering temperature of ϵ -Fe₂O₃ is ~ 500 K, i.e., well below that of other iron oxides such as hematite, magnetite or maghemite. Upon heating from room temperature, the saturation magnetization of ϵ -Fe₂O₃ nanoparticles undergoes a monotonic decrease while the coercivity and remanence sharply drop, virtually vanishing around ~ 500 K. However, above that temperature the hysteresis loops present a non-linear response with finite coercivity, evidencing signs of ferrimagnetic order up to temperatures as high as 850 K (T_{N1}). The neutron diffraction study confirms the presence of ferrimagnetic order well above 500 K with Pna'2₁' magnetic symmetry, but only involving two of the four Fe³⁺ sublattices which are ordered below $T_{N2} \approx 480$ K, and with a reduced net ferromagnetic component, that vanishes at above 850 K. The results unambiguously show the presence of a high-temperature magnetic phase in ϵ -Fe₂O₃ with a critical temperature of $T_{N1} \sim 850$ K. Importantly, this temperature is similar to the Curie point in other iron oxides, indicating comparable magnetic coupling strengths. The presence of diverse magnetic phases is further supported by the non-monotonic evolution of the thermal expansion. The existence of a high-temperature ferrimagnetic phase in ϵ -Fe₂O₃ may open the door to further expand the working range of this multifunctional iron oxide.

I. INTRODUCTION

Iron oxides constitute an exceptional family of materials that have been studied for many decades, because they present fundamental interest and proved and promising applicability for new technologies based on biochemical, magnetic, catalytic or multiferroic properties.¹⁻⁴

Apart from the amorphous Fe_2O_3 , Iron (III) oxide shows four known polymorph crystal structures: α - Fe_2O_3 (hematite), β - Fe_2O_3 and γ - Fe_2O_3 (maghemite) and ϵ - Fe_2O_3 .⁵ While hematite is the most common phase, ϵ - Fe_2O_3 is the most elusive and one of the less studied polymorphs. This is because its formation requires the mutually exclusive conditions of high temperatures and small sizes.⁶⁻⁸ The use of sol-gel methods with Si alcoxides and Fe salts made it possible to confine Fe_2O_3 nanoparticles in a silica matrix to prevent their growth while annealed above 1000°C, allowing, for the first time, to obtain virtually pure ϵ - Fe_2O_3 , opening the door to the study of this rare polymorph.⁹⁻¹¹ The structural characterization evidenced a complex non-centrosymmetric $Pna2_1$ structure isomorphous to the multiferroic GaFeO_3 , with four Fe sites in the asymmetrical unit: three in octahedral and one in tetrahedral environments.⁸ The magnetic studies revealed an unexpected huge room temperature coercivity: 20 kOe, making it the transition metal oxide with the highest coercivity and an appealing material for the next-generation high-density magnetic recording media, high-frequency electromagnetic wave absorbers or a building block for exchange coupled permanent magnets.¹²⁻¹⁵ Moreover, other important functionalities of ϵ - Fe_2O_3 are related with its magnetoelectric¹⁶ and multiferroic properties.⁴ These properties, quite unique among single metal oxides, stem from the structural features specific to this polymorph, in spite of being considered a structural intermediate between α - Fe_2O_3 and γ - Fe_2O_3 . Its structure produces a rich temperature-dependent diagram of magnetic phases. Between $T_C = 500$ K and $T_{N2} = 150$ K, ϵ - Fe_2O_3 exhibits a collinear ferrimagnetic structure due to the antiferromagnetic (AF) coupling (parallel to the a -axis) between dissimilar magnetic sublattices. This oxide then presents a broad low-temperature incommensurate magnetic transition starting at 150 K (ICOM1)¹⁷⁻¹⁸, characterized by a large reduction of the coercivity, the remanent and the saturation magnetization¹⁷. Under further cooling, below $T_{N3} \approx 85$ K, a second incommensurate magnetic order (ICOM2) takes place.¹³ Noticeable anomalies in the dielectric permittivity were reported in conjunction with these two successive transitions¹⁶. In addition, significant magnetostriction effects were observed in the interval 85-150 K where magnetic changes take place and spin-lattice coupling brings about atomic shifts within the

orthorhombic cell and a non-monotonous evolution of the Fe-O bonds¹⁹. A nonzero orbital magnetic moment ($m_L \sim 0.15 \mu_B/\text{Fe}$ at RT under 40 kOe) was detected by x-ray magnetic circular dichroism (XMCD) in the hard collinear ferrimagnetic phase ($150 \text{ K} < T < 490 \text{ K}$), which is suppressed by the magnetostructural changes concurrent with the magnetic transitions within the 85-150 K interval.¹⁵ On cooling, the coercive field drops in that interval from 20 kOe to 0.8 kOe, and then increases again under further cooling in the low-temperature magnetic phase (ICOM2), below 85 K.¹⁴ Likewise, a reentrant behavior of the orbital moment was also monitored by XMCD in the low temperature magnetic phase.¹⁴ The concurrent magnetostructural changes in the coordination polyhedra around Fe^{3+} sites and the reentrant evolution of the orbital moment should be seen as the signature of a relevant spin-orbit coupling in this magnetoelectric compound. Finally, the RT coexistence of ferrimagnetism and ferroelectricity, albeit with a small magnetocapacitance response, in thin epitaxial films of $\epsilon\text{-Fe}_2\text{O}_3$ further highlights the relevance of magnetoelastic couplings in this system, for which possible multiferroic properties in bulk form are still a subject of debate.

Importantly, although the Curie temperature of $\epsilon\text{-Fe}_2\text{O}_3$ has been postulated as $T_C \sim 500 \text{ K}$,^{3, 11, 20-23} no systematic studies of the magnetic properties above this temperature can be found in the literature.

Using diffraction and magnetometry techniques, we have investigated the magnetic and magnetostructural properties of $\epsilon\text{-Fe}_2\text{O}_3$ nanoparticles at high temperatures ($T > 500 \text{ K}$). The results evidence that contrary to the established scenario, $\epsilon\text{-Fe}_2\text{O}_3$ remains ferrimagnetic up to at least $T = 850 \text{ K}$, although with a reduced magnetization and a moderate coercivity.

II. EXPERIMENTAL DETAILS

In order to have a good signal to noise ratio in neutron diffraction studies it is desirable to perform measurements using more than 1.5 g of $\epsilon\text{-Fe}_2\text{O}_3$ (ideally obtained in a single synthesis). Thus, we prepared a silica gel containing 28 wt.% Fe_2O_3 from an hidroethanolic sol of tetraethyl orthosilicate (TEOS) of molar composition $\text{TEOS}:\text{Ethanol}:\text{water}=1:5:6$ containing dissolved iron nitrate nonahydrate. First, 5.4 ml of milliQ water and 26 ml of absolut ethanol (Panreac) were added to a 100 ml beaker and stirred for 5 min. Then, the 10.60 g of iron nitrate (Aldrich) were dissolved and the solution which attained a pH ~ 0.35 . Finally 20 ml of TEOS (Aldrich) were added dropwise to the solution under stirring ($\sim 200 \text{ rpm}$). The stirring, with the beaker covered, was maintained for 20 minutes after adding the TEOS. The sol was then distributed in 6 cm diameter petri dishes, attaining a level of 2-4

mm, which were placed in a plastic box, closed with its cover but not hermetically sealed, and placed in chemical hood at 23 °C. Gelation took place in about two weeks. The gels were removed from the petri dishes, allowed to dry and subsequently grinded in a ceramic mortar to be further dried at 60 °C in a stove. Then the xerogels were placed in an alumina boat and treated in a tubular furnace in air atmosphere at 200°C/h to 450°C and then to 1100°C at 80 °C/h, and were held for 3 h at this temperature before being cooled to room temperature at 350 °C/h. About 7.5 g of SiO₂/ε-Fe₂O₃ composite were obtained. The resulting material consisted of single crystalline ε-Fe₂O₃ nanoparticles embedded in a silica matrix with an average diameter of around 20 nm as observed by transmission electron microscopy. The silica was etched in hot (80°C) concentrated NaOH aqueous solution (12 M). For this purpose a round bottomed flask was filled with 180 ml of distilled water in which 76 g NaOH were dissolved, then about 5 g of SiO₂/ε-Fe₂O₃ composite were added to it and stirred overnight in a hot plate set at 80 °C using a water refrigerated condenser to avoid evaporation of water and a silicone oil bath to maintain an homogeneous temperature around the flask. Then the suspension was centrifuged at 6000 rpm for 2 min and the supernatant was discarded. The collected solid was re-dispersed in water and the centrifugation was repeated twice. Finally the tubes used for centrifugation were placed in a stove at 60°C and about 1.5 g of ε-Fe₂O₃ nanoparticles were collected after drying.

The quality of the samples was assessed by transmission electron microscopy, magnetic measurements and x-ray diffraction, as reported earlier^{6, 17}. Synchrotron x-ray powder diffraction patterns (SXRPD) were collected at the BL04-MSPD beamline²⁴ of the ALBA Synchrotron Light Facility (Barcelona, Spain) using $\lambda = 0.41284(6)$ Å. Patterns were recorded every 90 s by the MYTHEN position sensitive detector while warming the sample from 300 up to 923 K at a rate of 3 K/min. The working temperature was set using a CYBERSTAR hot air blower. Neutron powder diffraction (NPD) patterns were collected using the high-intensity, high-resolution D2B diffractometer of the Institute Laue-Langevin (ILL, Grenoble), between room temperature (RT) and 850 K ($\lambda = 1.594$ Å). Structural and magnetic Rietveld refinements were carried out using the Fullprof program²⁵. Crystallographic tools from the Bilbao Crystallographic server²⁶⁻²⁸ and ISOTROPY Software Suite²⁹ were also used.

The magnetic characterization, using dc and ac magnetic fields, was performed with the as-prepared ε-Fe₂O₃ nanoparticles embedded in SiO₂, using a Superconducting Quantum Interferometer Device (SQUID) and a Vibrating Sample Magnetometer (VSM) in a Physical Properties Measuring System (PPMS) both from Quantum Design. For the VSM

measurements the ϵ -Fe₂O₃/SiO₂ material was mixed with a high-temperature alumina cement. The use of ϵ -Fe₂O₃/SiO₂ composite instead of ϵ -Fe₂O₃ was necessary to avoid the transformation of ϵ -Fe₂O₃ to magnetite due to high temperatures and the vacuum environment during the measurements. The ac-susceptibility measurements were performed at 30 Hz and 1 kHz with a magnetic field amplitude of 4 Oe from 300 K to 750 K. The temperature dependence of the magnetization, *M*, was studied after zero field cooled (ZFC) and FC conditions under a dc field of 1 kOe from 300 to 900 K. Hysteresis loops were obtained between 900K and 300 K with a maximum applied magnetic field of 70 kOe.

III. RESULTS AND DISCUSSION

First it is worth emphasizing that the orthorhombic *Pna2₁* structure was stable up to the highest temperature reached (923 K). Namely, no transition to other more stable iron oxides (e.g., α -Fe₂O₃ or γ -Fe₂O₃) has been observed up to that temperature. The structural parameters of ϵ -Fe₂O₃ and agreement factors from the refinement of SXRPD patterns obtained at 305 K and 510 K can be seen in Table I. Figure 1(a) displays a projection of the ϵ -Fe₂O₃ non-centrosymmetric *Pna2₁* structure, composed of four different Fe sites in the asymmetrical unit cell, three octahedral and one tetrahedral environments. The coordination octahedra Fe1O₆ and Fe2O₆ are largely distorted, Fe3O₆ is a regular octahedron and Fe4O₄ is the tetrahedron. For clarity we will use the Fe1d, Fe2d, Fe3r, Fe4t atomic labels where "d", "r" and "t" refer to "*distorted*", "*regular*" and "*tetrahedral*" polyhedral coordination, respectively.

The presence of very minority impurities was carefully explored by a detailed examination of high intensity synchrotron patterns. We detected a 2.3(9)% in weight of α -Fe₂O₃ (hematite) as impurity phase in our nanograin ceramic samples of ϵ -Fe₂O₃ (corresponding to the bottom row of bars in the refined synchrotron pattern shown in Fig. 1(b)). This corresponds to a 0.7 wt. % in the SiO₂/Fe₂O₃ composite used for magnetic measurements.

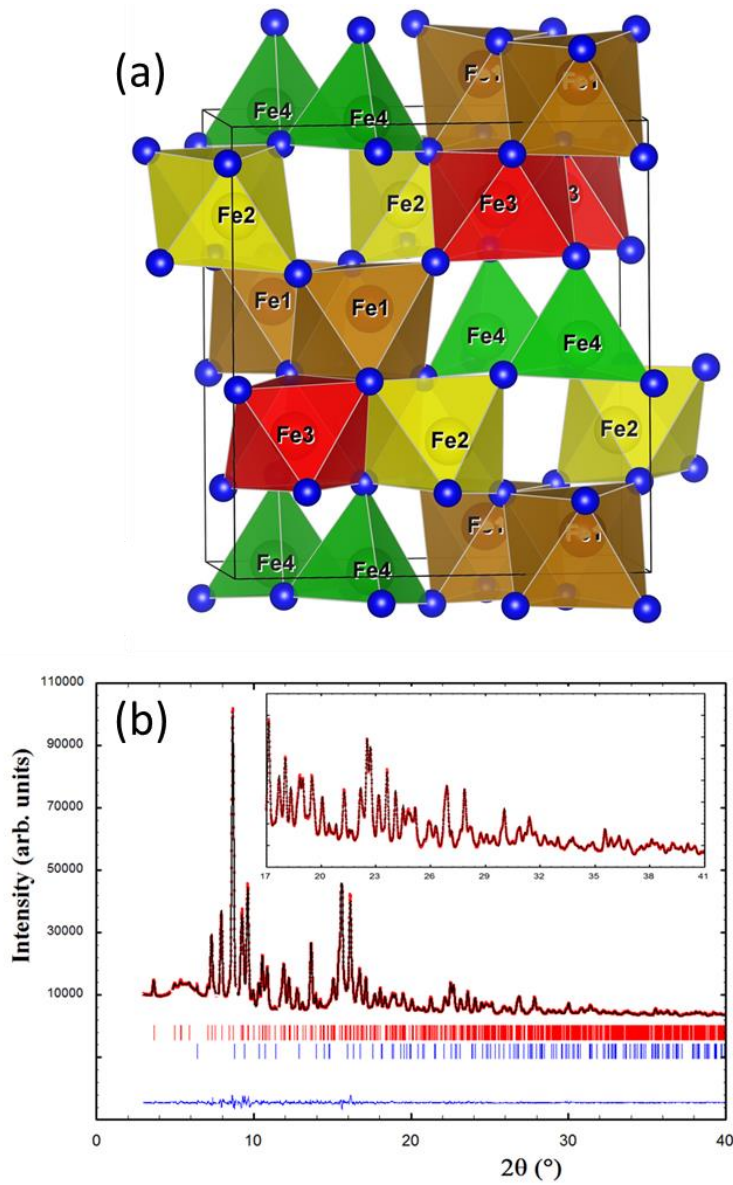


Figure 1. (a) Crystallographic projection of ϵ - Fe_2O_3 . The four crystallographically independent Fe sites are shown with different colors in the structure (Fe1, brown; Fe2 yellow; Fe3 green; Fe4 red). O atoms are represented in dark blue. (b) Rietveld refinement (black solid line) of the synchrotron x-ray pattern of ϵ - Fe_2O_3 collected at 300K (red circles: experimental points; bottom blue line: difference). The top row of bars (in red) corresponds to ϵ - Fe_2O_3 , while the bottom row (in blue) is for hematite (α - Fe_2O_3 , 2% weight). The inset shows an enlarged view of the high-angle region.

III-a Magnetometry

The temperature dependence of the ZFC and FC magnetization of the ϵ - Fe_2O_3 particles embedded in SiO_2 is plotted in Fig. 2(a). Two ferrimagnetic regimes with very different magnetic behavior can be clearly distinguished below and above ~ 500 K (denoted FM2 and FM1 respectively). Remarkably, contrary to the scenario assumed in previous reports, the

ferrimagnetic FM2 phase does not become paramagnetic above 500 K. The $M(T)$ evolution in Fig. 2 reveals a second phase transition, evidencing the existence of a new ferrimagnetic state (FM1) between 500 K and ~ 850 K. The transition temperature between FM1 and FM2 can be established at $T_{N2} = 480$ K by the lambda-shaped peak in the ac susceptibility vs temperature curve presented in the inset of Fig. 2(a). From the hysteresis loops at $T > 500$ K it can be clearly seen that FM1 presents a ferromagnetic behavior with finite net magnetic moment and coercivity, H_C .

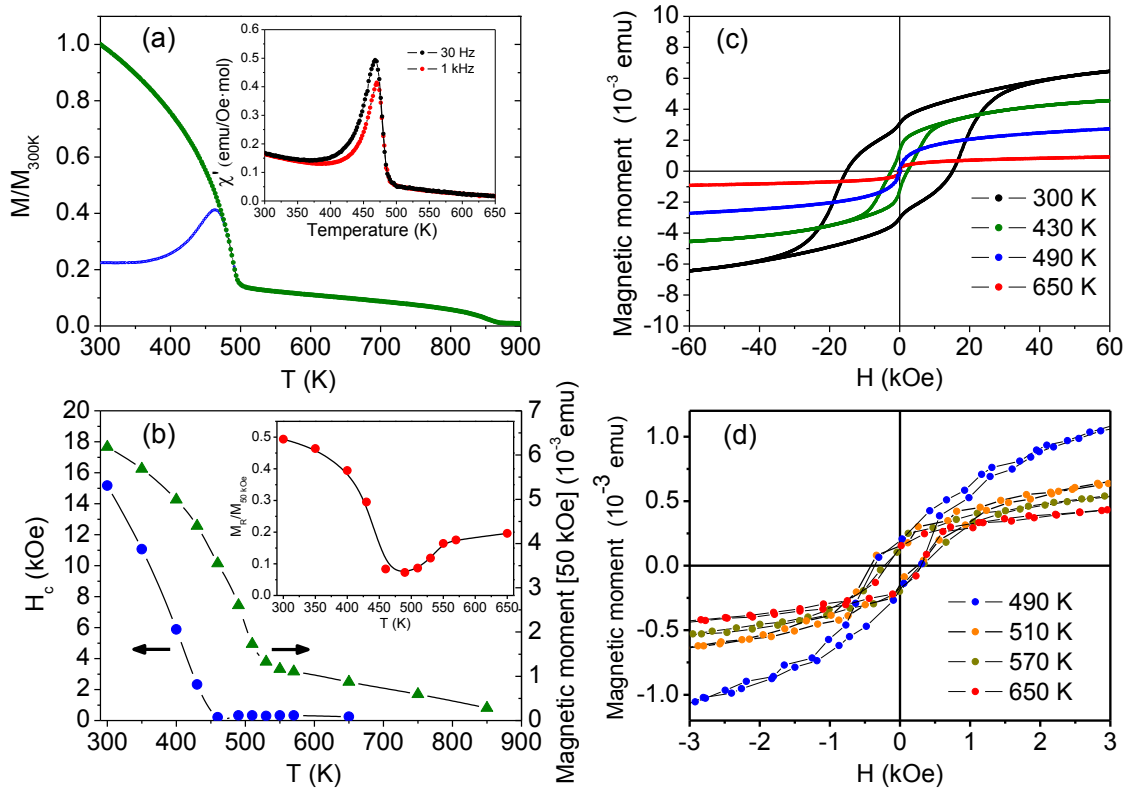


Figure 2. (Color online) (a) FC (green) and ZFC (blue) dc magnetization curves (1 kOe) of the ϵ - Fe_2O_3 nanoparticles embedded in SiO_2 between 300 and 900 K. Inset: real part of the ac-susceptibility ($h=4$ Oe). (b) Temperature evolution of the coercive field (H_C ; left axis) and net magnetic moment at 50 kOe ($M[50\text{kOe}]$; right axis). Inset: dependence of the $M_r/M[50\text{kOe}]$ ratio. Hysteresis loops characteristic of (c) the FM2 phase and (d) the FM1 phase (note the different x- and y-scales in both figures, and the loops at 490 K and 650 K included in both panels for the sake of comparison).

However, as can be seen in Fig. 2(b) there is a drastic collapse of the large H_C (characteristic of FM2) and $M[50\text{ kOe}]$ at $T_{N2} = 480\text{ K}$ (see Figs. 2(b)(c)). Moreover, upon heating, $M[50\text{ kOe}]$ undergoes a Brillouin-type monotonic decrease up to 550 K, although the coercivity (and remanence, M_r) sharply drop well before this temperature, having practically vanished around ~ 480 K. Nevertheless, although H_C shrinks by more than a factor 10 from $H_C \sim 16$

kOe at RT, it remains moderate (~ 400 Oe) even at $T \gg 500$ K (T_{N2}) (see Fig. 2(d)). Importantly, from the evolution of the magnetic properties it can be established that the critical temperature of the FM1 phase is about $T_{N1} \sim 850$ K. Hence, although there is a drastic breakdown of the hard ferrimagnetic state at $T_{N2} = 480$ K, it does not give rise to a paramagnetic phase, but it is transformed into a new softer ferrimagnetic state.

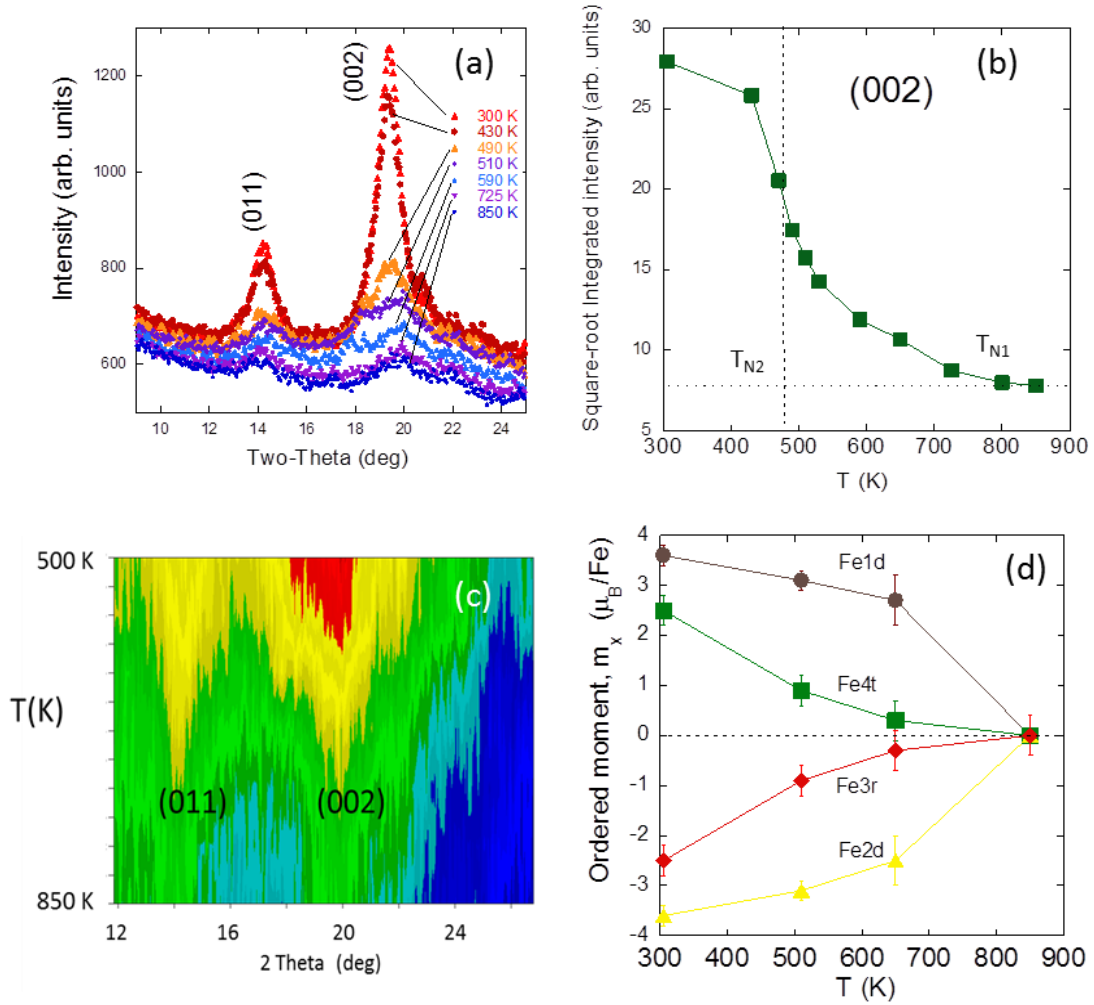


Figure 3. (a) Neutron patterns at selected temperatures in the range comprising the main magnetic peaks (011) and (002). (b) Square-root of the neutron integrated intensity of the strongest magnetic reflection (002). (c) Evolution of the neutron diffraction intensities above T_{N2} for the characteristic magnetic reflections. (d) Evolution of the ordered magnetic moments refined at Fe1d (brown), Fe2d (yellow), Fe3r (red) and Fe4t (green) sites in the structure.

III-b Neutron diffraction study of the successive ferrimagnetic phases

To better understand the nature of the very high-temperature ferrimagnetic phase a systematic NPD study was performed.

As can be seen in Fig. 3(a), the intensity of the magnetic peaks (011) and (002) progressively decreases as the temperature is increased from RT to 850 K. In agreement with the magnetization results, the intensity of the magnetic peaks remains finite even far above T_{N2} . However, the temperature dependence of the integrated intensity of the (002) peak (proportional to the ordered moment), shown in Fig. 3(b), strongly differs from a Brillouin-type evolution and exhibits the shape of a long magnetic tail that persists far beyond T_{N2} .

The magnetic structures and atomic ordered moments were fully analyzed using the neutron diffraction patterns at the two selected temperatures 305 K and 510 K. The former being representative of the ferrimagnetic phase FM2, and the second (above but close to $T_{N2} = 480$ K) of the new ferrimagnetic phase FM1. Note that the magnetic reflections detected between $T_{N2}(=480$ K) and $T_{NI}(\sim 850$ K) do not indicate changes in the extinction conditions or the translational symmetry.

Possible magnetic or Shubnikov space groups compatible with the $Pna2_1$ symmetry and null magnetic propagation vector $\mathbf{k} = 0$ were considered. It was found that the magnetic ordering adopts the same magnetic space group in the two ferrimagnetic phases, $Pna'2_1'$ [# 33.147, transformation to standard settings: $(\mathbf{a}, \mathbf{b}, \mathbf{c}; 0, 0, 0)$]^{25,27}. The Rietveld refinement of neutron patterns at 305 K (FM2 magnetic phase) and 510 K (FM1 magnetic phase) are plotted in Figure 4 and the results are summarized in Table II.

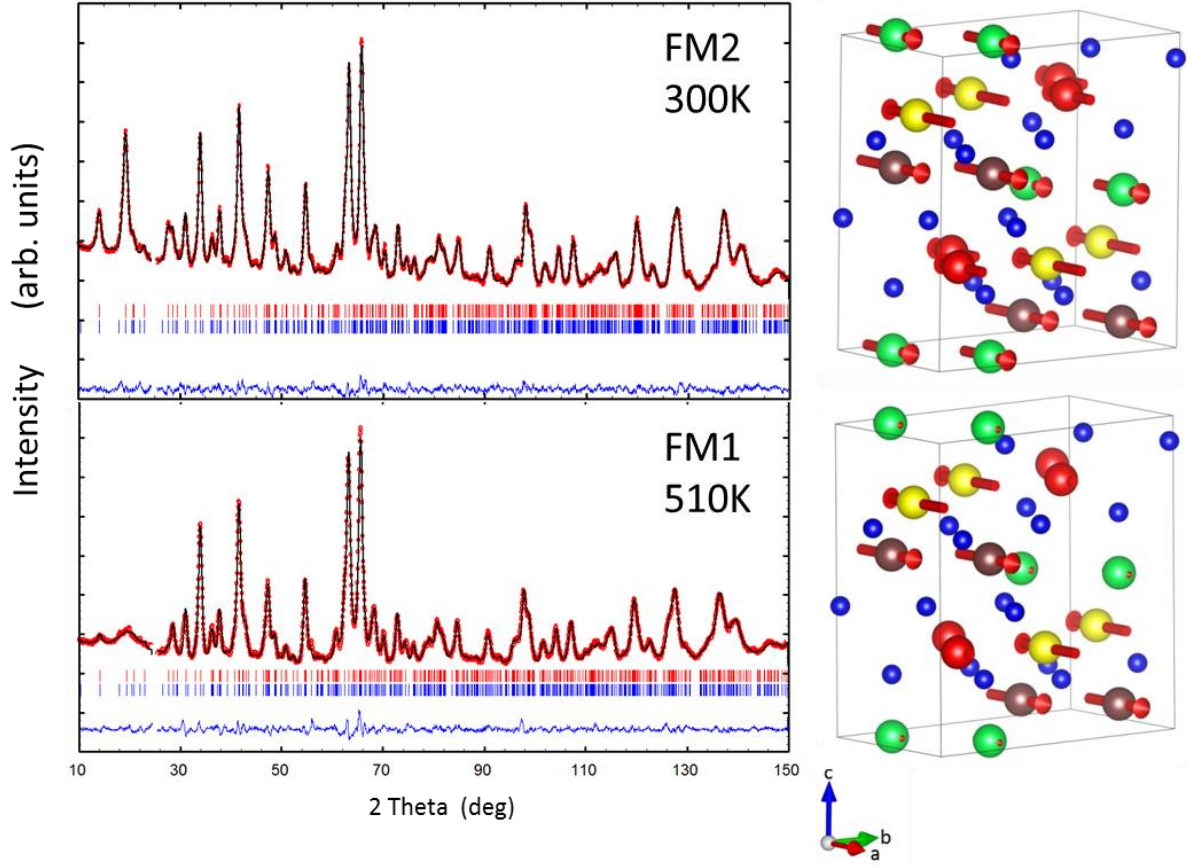


Figure 4. (Color online) Neutron Rietveld refinement (black line) of the NPD patterns for ϵ -Fe₂O₃ obtained at 305 K ($T < T_{N2}$, FM2 ordering) and 510 K ($T_{N2} < T < T_{N1}$, FM1 ordering) (D2B, red circles: experimental points; bottom blue line: difference). Upper row of reflections correspond to the $Pna2_1$ structure, the lower one to the magnetic ordered phase ($Pna'2_1$). Goodness factors at 305 K (510K): $R_B=2.2$ 2.48(1.8), $R_f=1.3$ 1.55(1.1), $R_{Mag}=2.2$ 2.92(1.2), $\chi^2=1.27$ 0.31 (3.5). (Right) Schematic view of the FM1 (bottom) and FM2 (top) magnetic ordering at the same temperatures. Fe1d (brown), Fe2d (yellow), Fe3r (red) and Fe4t (green); O (dark blue).

Interestingly, despite the abrupt drop in the displayed by magnetization at T_{N2} , there are ordered magnetic moments with very large m_x components that steadily persist in the interval $T_{N2}(=480 \text{ K}) < T < T_{N1}(=850 \text{ K})$ (m, magnetic moment). Nevertheless, they are found selectively in Fe1d and Fe2d octahedral sites. These two Fe positions are magnetically robust and persist antiferromagnetically coupled above T_{N2} . Their antiparallel ordered moments as refined at intermediate temperatures have been plotted in Fig. 3(d). Remarkably, the main difference detected between FM2 and FM1 orders concerns the high degree of magnetic disorder at the Fe3rO6 and Fe4tO4 sites. Neutron data did not allow us discern ordered moments at Fe3r and Fe4t sites independently, and their moments were kept (above T_{N2}) identical and antiparallel, forcing $m_x[\text{Fe3r}] = -m_x[\text{Fe4t}]$, in the neutron refinements. The

refined m_x moments at these positions are also displayed in the Fig. 3(d), which shows the evolution of the ordered moments (m_x) refined for the four Fe sites. In the high temperature phase the difference between the moments in one antiparallel pair (e.g. Fe3r/Fe4t) is smaller than our experimental error. At RT (305 K) the resultant net uncompensated moment $\sim 0.2 \mu_B/\text{Fe}$ (i.e. 14 emu/g) is in agreement with M_s values (net ferromagnetic signal) previously reported^{10, 17}. Therefore, at the FM2/FM1 (hard/soft) ferrimagnetic phase boundary, there is a clear disruption of the magnetic order of the iron spins occupying the tetrahedral Fe4t and the undistorted octahedral Fe3r sites. The small moment values refined at 510 K indicate that Fe3r and Fe4t sublattices are practically disordered above T_{N2} . Likewise, the onset of magnetic ordering near 850 K is essentially driven by the AFM coupling of Fe spins in the more distorted octahedral positions (Fe1d and Fe2d). Fig. 3(d) clearly illustrates the anomalous evolution of the ordered moments at Fe3r/Fe4t sites. Most likely this evolution is the result of strong frustration effects between sublattices, which can be identified by the broad magnetic reflections at high temperatures.

Using a molecular-field model, the appearance of spontaneous magnetization in the FM2 phase of $\epsilon\text{-Fe}_2\text{O}_3$ has been associated with the lower superexchange $Z_{ij}J_{ij}$ values of the tetrahedral site, compared to those of octahedral sites.²² As can be seen in Fig. 3d the ordered moments at the Fe1d and Fe2d sites are larger than in the Fe4t tetragonal site in the whole range above room temperature, in concordance with the theoretical predictions. On another hand, our neutron diffraction results establish that the abrupt enhancement of the magnetization below T_{N2} takes place concurrently with the long-range ordering of Fe4t magnetic atoms occupying the tetrahedral site.

Interestingly, the new ferrimagnetic-paramagnetic boundary is shifted towards the upper characteristic ordering temperatures of ferrimagnetic iron oxides, 950 K for $\alpha\text{-Fe}_2\text{O}_3$, 940 K for $\gamma\text{-Fe}_2\text{O}_3$ and 853 K for Fe_3O_4 , indicating that $\epsilon\text{-Fe}_2\text{O}_3$ presents comparable magnetic coupling strengths. Notably, the NPD analysis unambiguously demonstrates that the ordered magnetic components are associated to $\epsilon\text{-Fe}_2\text{O}_3$, ruling out the possibility that the magnetic response above 480 K might be due to impurities of the ferrimagnetic oxides mentioned above, which present a completely different set of magnetic reflections (see Fig. S1 of the Supplementary Material). Additionally, the fact that some of the magnetic peaks, although very broad, remain finite at 850 K may indicate the possible existence of a frustrated (with no long-range order) ferrimagnetic phase even above T_{N1} , similar to other oxide systems.³⁰

III-c Magneto-structural coupling at the ferrimagnetic transitions studied using synchrotron x-ray diffraction

Magnetic ordering at high temperatures in ε -Fe₂O₃ concurs with significant magnetostructural and thermal expansion anomalies, as shown by the evolution of the orthorhombic cell obtained from SXRPD (Figure 5). The cell volume reveals an abrupt contraction ($\approx 0.1\%$) at about 500 K upon cooling from high temperature (Fig. 5(a)) with the appearance of the hard FM2 phase. The anomaly is also visible in the evolution of all three $a(T)$, $b(T)$ and $c(T)$ cell parameters (Fig. 5(b)): a and b abruptly contract and c expands when Fe3r and Fe4t spins become long-range ordered (T_{N2}).

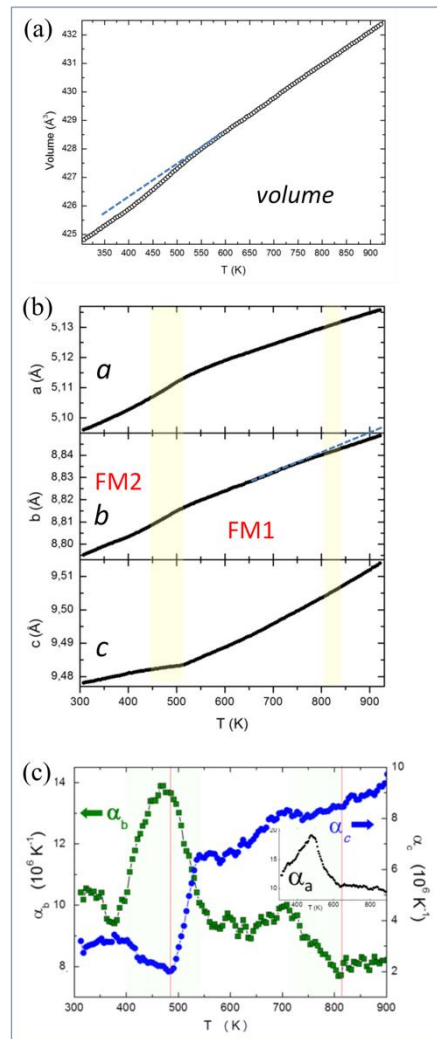


Figure 5. (a) Evolution of the unit-cell volume above room temperature obtained from SXRPD data. (b) Temperature dependence of the orthorhombic cell parameters in the 300-925 K range showing magnetostructural anomalies associated to the emergence of the FM1 and FM2 ferrimagnetic orders. (c) The linear thermal expansion coefficient α_i ($i=b$ and c) derived from SXRPD data and $a_i(T)$ as $\alpha_i = 1/l_{i0} \times dl_i/dT$. The temperature dependence of the coefficients $\alpha_b(T)$ and $\alpha_c(T)$ are shown on the left- and right-axis respectively. Inset: $\alpha_a(T)$.

In the Fig. 5(c) we plot the linear thermal expansion coefficients α , deduced from $\alpha_i(T)$ as $\alpha_i = 1/l_{i0} \times dl_i/dT$ ($l_i : a, b, c$), where l_{i0} is the value of the l_i parameter (size of the unit cell along $i: a, b, c$) at 305 K. Interestingly, there are anomalous contributions to the lattice evolution which are concurrent with the magnetic transitions. On the one hand, the most prominent exchange-striction effects come up accompanying the hard/soft ferrimagnetic phase boundary (Fig. 2). Similarly, the evolution of $\alpha_b(T)$ in Fig. 5(c) also shows a significant anomaly in the range 700-825 K which could be caused by the appearance of magnetic order at Fe1d and Fe2d sites in the FM1 phase, which is in concordance with the small deviation observed in $b(T)$ near ~800 K (Fig. 5(b)). Note that the exchange-striction effect at T_{N1} provides further evidence that the magnetic properties between 480 K and 850 K do not originate from impurities, but from the FM1 phase of ϵ -Fe₂O₃.

In this way, although both ferrimagnetic phases exhibit the same magnetic space group ($Pna'2_1'$ (n. 33.147)) and moment orientation (parallel to a), the observed magnetostructural response is very different in both transitions. The origin of these differences should correlate with the dissimilar character of each of the phases (i.e., fully ordered FM2 vs partially frustrated FM1).

IV. CONCLUDING REMARKS

In the preceding sections we have investigated the puzzling magneto-structural properties of polycrystalline ϵ -Fe₂O₃ above room temperature. Contrary to the scenario proposed in the literature, magnetic order in this magnetoelectric Iron (III) polymorph does not disappear at the hard-ferrimagnetic transition near 480 K. We have shown that a second ferrimagnetic phase (FM1) persists up to much higher temperatures (near 850 K). The hard ferrimagnetic FM2 phase (holding giant coercivity presumably stimulated by a nonzero orbital angular moment) is transformed to a different ferrimagnet state, FM1, with a much smaller ferromagnetic component and coercivity. Both magnetic orders adopt the magnetic space group $Pna'2_1'$ (n. 33.147), where the main difference between them is the disruption of the magnetic order associated to the Fe3r and Fe4t magnetic atoms. Above 480 K, the iron spins at the sublattices that occupy the regular octahedra Fe3O₆ and Fe4O₄ tetrahedra can hardly keep their antiparallel magnetizations and become rapidly disordered. Consequently, the spontaneous FM magnetization that was sustained by the

different magnetic moments in these antiparallel sublattices in FM2 quickly vanishes in FM1. Thus, the small FM component persisting up to $T_{NI} \approx 850$ K results from a slightly dissimilar magnetization at the antiparallel Fe1d and Fe2d sublattices. Hence, we have demonstrated that the ferrimagnetic-paramagnetic phase boundary in ϵ -Fe₂O₃ is $T_{NI} \sim 850$ K. This temperature is similar to the Curie point in other iron oxides, confirming comparable magnetic coupling strengths. This may open the door to further expand the working range of this multifunctional iron oxide. In fact, these new findings may be an indication that the presumed multiferroic properties of ϵ -Fe₂O₃ at room temperature actually could persist and extend also into the new ferrimagnetic FM1 phase.

ACKNOWLEDGMENTS

We thank financial support from the Spanish Ministry of Economy and Competitiveness, through projects MAT2015-686760-02-2-P, MAT2012-38213-C02-02, MAT2016-77391-R and “Severo Ochoa” Programme for Centres of Excellence in R&D (SEV- 2015-0496 and SEV-2013-0295). The formers are co-funded by ERDF of European Union. The Generalitat de Catalunya is also acknowledged for financial support (projects 2014SGR213 and 2014SGR1015). ICN2 is funded by the CERCA Programme/Generalitat de Catalunya. We also acknowledge ILL and ALBA for granting beamtime. C. Ritter is acknowledged for technical assistance during neutron measurements. J.L.G-M thanks J. M. Pérez-Mato for fruitful discussions. Ana Arauzo, from the Physical Measurements service at University of Zaragoza is acknowledged for performing ac susceptibility measurements.

REFERENCES

1. Cornell, R. M.; Schwertmann, U., Applications. In *The Iron Oxides*, Wiley-VCH Verlag GmbH & Co. KGaA: 2004; pp 509-524.
2. Carraro, G.; Maccato, C.; Gasparotto, A.; Montini, T.; Turner, S.; Lebedev, O. I.; Gombac, V.; Adami, G.; Van Tendeloo, G.; Barreca, D.; Fornasiero, P., Enhanced Hydrogen Production by Photoreforming of Renewable Oxygenates Through Nanostructured Fe₂O₃ Polymorphs. *Adv. Funct. Mater.* **2014**, *24*, 372-378.
3. Tucek, J.; Zboril, R.; Namai, A.; Ohkoshi, S., ϵ -Fe₂O₃: An Advanced Nanomaterial Exhibiting Giant Coercive Field, Millimeter-Wave Ferromagnetic Resonance, and Magnetoelectric Coupling. *Chem. Mater.* **2010**, *22*, 6483-6505.
4. Gich, M.; Fina, I.; Morelli, A.; Sánchez, F.; Alexe, M.; Gàzquez, J.; Fontcuberta, J.; Roig, A., Multiferroic Iron Oxide Thin Films at Room Temperature. *Adv. Mater.* **2014**, *26*, 4645-4652.
5. Zboril, R.; Mashlan, M.; Petridis, D., Iron(III) oxides from thermal processes- synthesis, structural and magnetic properties, Mossbauer spectroscopy characterization, and applications. *Chem. Mater.* **2002**, *14*, 969-982.
6. Gich, M.; Roig, A.; Taboada, E.; Molins, E.; Bonafos, C.; Snoeck, E., Stabilization of metastable phases in spatially restricted fields: the case of the Fe₂O₃ polymorphs. *Faraday Discuss.* **2007**, *136*, 345-354.
7. Sakurai, S.; Namai, A.; Hashimoto, K.; Ohkoshi, S., First Observation of Phase Transformation of All Four Fe₂O₃ Phases ($\gamma \rightarrow \epsilon \rightarrow \beta \rightarrow \alpha$ -Phase). *J. Am. Chem. Soc.* **2009**, *131*, 18299-18303.
8. Tadic, M.; Milosevic, I.; Kralj, S.; Mitric, M.; Makovec, D.; Sabounji, M. L.; Motte, L., Synthesis of metastable hard-magnetic ϵ -Fe₂O₃ nanoparticles from silica-coated akaganeite nanorods. *Nanoscale* **2017**, *9*, 10579-10584.
9. Tronc, E.; Chaneac, C.; Jolivet, J. P., Structural and magnetic characterization of ϵ -Fe₂O₃. *J. Solid State Chem.* **1998**, *139*, 93-104.
10. Jin, B.; Ohkoshi, S.; Hashimoto, K., Giant coercive field of nanometer-sized iron oxide. *Adv. Mater.* **2004**, *16*, 48-51.
11. Popovici, M.; Gich, M.; Niznansky, D.; Roig, A.; Savii, C.; Casas, L.; Molins, E.; Zaveta, K.; Enache, C.; Sort, J.; de Brion, S.; Chouteau, G.; Nogues, J., Optimized synthesis of the elusive ϵ -Fe₂O₃ phase via sol-gel chemistry. *Chem. Mater.* **2004**, *16*, 5542-5548.
12. Namai, A.; Sakurai, S.; Nakajima, M.; Suemoto, T.; Matsumoto, K.; Goto, M.; Sasaki, S.; Ohkoshi, S., Synthesis of an Electromagnetic Wave Absorber for High-Speed Wireless Communication. *J. Am. Chem. Soc.* **2009**, *131*, 1170-1173.
13. Namai, A.; Yoshikiyo, M.; Yamada, K.; Sakurai, S.; Goto, T.; Yoshida, T.; Miyazaki, T.; Nakajima, M.; Suemoto, T.; Tokoro, H.; Ohkoshi, S., Hard magnetic ferrite with a gigantic coercivity and high frequency millimetre wave rotation. *Nat. Commun.* **2012**, *3*, 1035.
14. Lopez-Ortega, A.; Estrader, M.; Salazar-Alvarez, G.; Roca, A. G.; Nogues, J., Applications of exchange coupled bi-magnetic hard/soft and soft/hard magnetic core/shell nanoparticles. *Phys. Rep.* **2015**, *553*, 1-32.
15. Hozumi, T.; Irie, S.; Chiba, T. Magnetic Material, Magnet and Method for Producing the Magnetic Material, WO2012/101752 A1. 02.08.2012, 2012.
16. Gich, M.; Frontera, C.; Roig, A.; Fontcuberta, J.; Molins, E.; Bellido, N.; Simon, C.; Fleta, C., Magnetoelectric coupling in ϵ -Fe₂O₃ nanoparticles. *Nanotechnology* **2006**, *17*, 687-691.

17. Gich, M.; Roig, A.; Frontera, C.; Molins, E.; Sort, J.; Popovici, M.; Chouteau, G.; Marero, D. M. Y.; Nogues, J., Large coercivity and low-temperature magnetic reorientation in ϵ -Fe₂O₃ nanoparticles. *J. Appl. Phys.* **2005**, *98*, 044307.
18. Gich, M.; Frontera, C.; Roig, A.; Taboada, E.; Molins, E.; Rechenberg, H. R.; Ardisson, J. D.; Macedo, W. A. A.; Ritter, C.; Hardy, V.; Sort, J.; Skumryev, V.; Nogues, J., High- and low-temperature crystal and magnetic structures of ϵ -Fe₂O₃ and their correlation to its magnetic properties. *Chem. Mater.* **2006**, *18*, 3889-3897.
19. Tseng, Y. C.; Souza-Neto, N. M.; Haskel, D.; Gich, M.; Frontera, C.; Roig, A.; van Veenendaal, M.; Nogues, J., Nonzero orbital moment in high coercivity ϵ -Fe₂O₃ and low-temperature collapse of the magnetocrystalline anisotropy. *Phys. Rev. B* **2009**, *79*, 094404.
20. Forestier, H.; Guiot-Guillain, G., A new ferromagnetic variety of iron sesquioxide. *C. R. Acad. Sci. (Paris)* **1934**, *199*, 720-723.
21. Schrader, R.; Buttner, G., A New phase of Iron (III)-oxide - ϵ -Fe₂O₃. *Z. Anorg. Allg. Chem.* **1963**, *320*, 220-234.
22. Ohkoshi, S.; Namai, A.; Sakurai, S., The Origin of Ferromagnetism in ϵ -Fe₂O₃ and ϵ -GaFe_{2-x}O₃ Nanomagnets. *J. Phys. Chem. C* **2009**, *113*, 11235-11238.
23. López-Sánchez, J.; Serrano, A.; Del Campo, A.; Abuín, M.; Rodríguez de la Fuente, O.; Carmona, N., Sol-Gel Synthesis and Micro-Raman Characterization of ϵ -Fe₂O₃ Micro- and Nanoparticles. *Chem. Mater.* **2016**, *28*, 511-518.
24. Fauth, F.; Boer, R.; Gil-Ortiz, F.; Popescu, C.; Vallcorba, O.; Peral, I.; Fullà, D.; Benach, J.; Juanhuix, J., The crystallography stations at the Alba synchrotron. *Eur. Phys. J. Plus* **2015**, *130*, 160.
25. Rodríguez-Carvajal, J., Recent Advances in Magnetic-Structure Determination by Neutron Powder Diffraction. *Physica B* **1993**, *192*, 55-69.
26. Aroyo, M. I.; Perez-Mato, J. M.; Capillas, C.; Kroumova, E.; Ivantchev, S.; Madariaga, G.; Kirov, A.; Wondratschek, H., Bilbao crystallographic server: I. Databases and crystallographic computing programs. *Z. Kristallogr.* **2006**, *221*, 15-27.
27. Aroyo, M. I.; Kirov, A.; Capillas, C.; Perez-Mato, J. M.; Wondratschek, H., Bilbao crystallographic server. II. Representations of crystallographic point groups and space groups. *Acta Crystallogr. A* **2006**, *62*, 115-128.
28. Perez-Mato, J. M.; Gallego, S. V.; Tasci, E. S.; Elcoro, L.; de la Flor, G.; Aroyo, M. I., Symmetry-Based Computational Tools for Magnetic Crystallography. *Annu. Rev. Mater. Res.* **2015**, *45*, 217-248.
29. Campbell, B. J.; Stokes, H. T.; Tanner, D. E.; Hatch, D. M., ISODISPLACE: a web-based tool for exploring structural distortions. *J. Appl. Crystallogr.* **2006**, *39*, 607-614.
30. Kuriki, A.; Moritomo, Y.; Xu, S.; Ohoyama, K.; Kato, K.; Nakamura, A., Diffuse scattering due to geometrical frustration in Mn₃O₄. *J. Phys. Soc. Jpn.* **2003**, *72*, 458-459.

Table I. Atomic coordinates of ϵ -Fe₂O₃ obtained from SXRPD at 300 K and 510 K.

	T=300 K			T=510 K		
Atoms	x	y	z	x	y	z
Fe1	0.1947(5)	0.1497(3)	0.5806(2)	0.1928(6)	0.1499(4)	0.5813(2)
Fe2	0.6828(3)	0.0323(2)	0.7921(3)	0.6823(4)	0.0314(2)	0.7918(3)
Fe3	0.8083(3)	0.1592(2)	0.3062(2)	0.8105(4)	0.1583(2)	0.3079(2)
Fe4	0.1816(5)	0.1538(3)	0.00000	0.1819(6)	0.1542(4)	0.00000
O1	0.9754(13)	0.3276(5)	0.4340(5)	0.9739(14)	0.3281(6)	0.4345(6)
O2	0.5112(13)	0.4933(8)	0.4187(9)	0.5030(14)	0.4907(9)	0.4227(13)
O3	0.6537(15)	1.0011(7)	0.1895(5)	0.6533(18)	0.9990(8)	0.1859(5)
O4	0.1624(14)	0.1622(8)	0.1956(4)	0.1614(16)	0.1608(8)	0.1959(4)
O5	0.8449(15)	0.1657(8)	0.6680(5)	0.8450(17)	0.1669(10)	0.6698(5)
O6	0.5286(13)	0.1590(9)	0.9375(6)	0.5386(14)	0.1654(10)	0.9366(7)
	a=5.0967(2) b=8.7953(3) c=9.4770(3)			a=5.1133(2) b=8.8163(4) c=9.4822(4)		

Agreement factors for SXRPD pattern at 300 K (510 K): $R_B=1.35(1.31)$, $R_F=1.04(1.01)$,
 $R_{Mag}=4.45(4.48)$, $\chi^2=4.6$ (4.8)

Table II. Magnetic groups and refined magnetic moments in the ferrimagnetic FM1 (T_{N1}) and FM2 (T_{N2}) phases. The d, r and t labels of the four iron sites refer to *distorted*, *regular* and *tetrahedral* polyhedra, respectively). The goodness factors are given in Fig. 3.

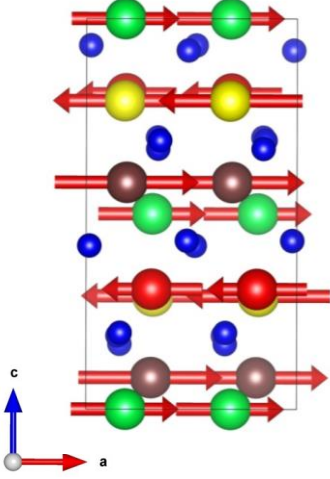
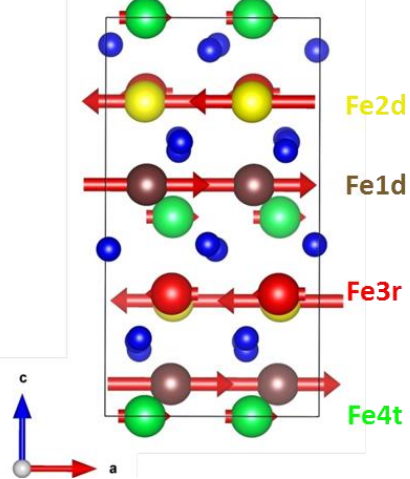
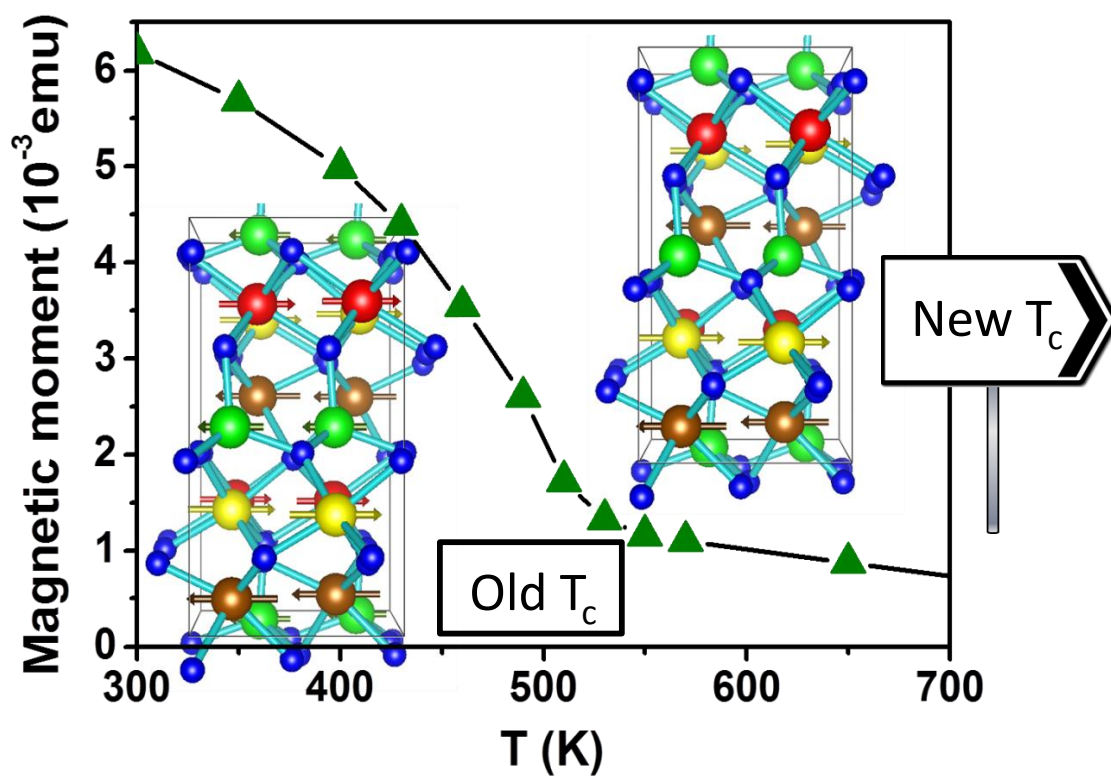
Temperature	300 K	510 K
Magnetic Space Group	$Pna'2_1'$ (n. 33.147)	$Pna'2_1'$ (n. 33.147)
Transformation to standard setting	(a, b, c; 0, 0, 0)	
Fe atoms in the asymmetric unit	Coordinates Expressed in parent Ort. setting: Fe1d \approx (0.193, 0.149, 0.581) Fe2d \approx (0.682, 0.031, 0.792) Fe3r \approx (0.809, 0.158, 0.307) Fe4t \approx (0.181, 0.153, 0.000)	
Magnetic phase	FM2	FM1
Refined moments	$m_x[\text{Fe1d}] = 3.6(1) \mu_B/\text{Fe}$ $m_x[\text{Fe2d}] = -3.6(1) \mu_B/\text{Fe}$ $m_x[\text{Fe3r}] = -2.5(1) \mu_B/\text{Fe}$ $m_x[\text{Fe4t}] = 2.7(3) \mu_B/\text{Fe}$	$m_x[\text{Fe1d}] = 3.1(1) \mu_B/\text{Fe}$ $m_x[\text{Fe2d}] = -3.1(1) \mu_B/\text{Fe}$ $m_x[\text{Fe3r}] = -0.9(2) \mu_B/\text{Fe}$ $m_x[\text{Fe4t}] = 0.9(3) \mu_B/\text{Fe}$
Magnetic structure		

Table of Contents



ASSOCIATED CONTENT

Supporting Information. Simulation of a neutron diffraction pattern of 50 wt. % ϵ - Fe_2O_3 and 50 wt. % α - Fe_2O_3 compared to the experimental pattern collected at 305 K. This material is available free of charge via the Internet at <http://pubs.acs.org>.